



XXXVII IBERIAN LATIN AMERICAN CONGRESS
ON COMPUTATIONAL METHODS IN ENGINEERING
BRASÍLIA - DF - BRAZIL

HIGH ORDER FINITE ELEMENT BASES FOR $H(\text{div})$ SPACES BASED ON 3D ADAPTIVE CURVED MESHES

Philippe R. B. Devloo

Omar Durán

Sônia M. Gomes

phil@fec.unicamp.br

omaryesiduran@gmail.com

soniag@ime.unicamp.br

Universidade Estadual de Campinas (FEC, FEM and IMECC)

Campinas, SP, Brazil

Nathan Shauer

nathan.sh@gmail.com

Civil & Environmental Engineering, University of Illinois Urbana-Champaign, USA

Abstract. *Two stable approximation space configurations are treated for discrete versions of the mixed finite element method for elliptic problems. The construction of these approximation spaces are based on curved 3D meshes composed of different topologies (tetrahedral, hexahedral or prismatic elements). Furthermore, their choices are guided by the property that, in the master element, the image of the flux space by the divergence operator coincides with the primal space. Additionally, by using static condensation, the global condensed matrices sizes, which are proportional to the dimension of border fluxes, are reduced, noting that this dimension is the same in both configurations. For uniform meshes with constant polynomial degree distribution, accuracy of order $k + 1$ or $k + 2$ for the primal variable is reached, while keeping order $k + 1$ for the flux in both configurations. The case of hp -adaptive meshes is treated for application to the simulation of the flow in a porous media around a cylindrical well. The effect of parallelism and static condensation in CPU time reduction is illustrated.*

Keywords: *Mixed finite elements, $H(\text{div})$ -conforming spaces, curved elements, hp -adaptivity*

1 INTRODUCTION

Mixed finite element formulations for elliptic problems are characterized by simultaneous calculations of the potential (primal variable) and of the flux field (dual variable) (Brezzi & Fortin, 1991). In addition to $\mathbf{H}(\text{div})$ -conforming finite element spaces for flux approximations, with continuous normal components over element interfaces, the primal variable is usually represented in discontinuous finite element spaces. If these approximation spaces are chosen properly, they have the ability to provide accurate and locally conservative fluxes, an advantage over standard H^1 -conforming finite element discretizations.

This work focuses on new $\mathbf{H}(\text{div})$ -conforming finite element spaces for flux approximations based on curved 3D meshes composed of different topologies (tetrahedral, hexahedral or prismatic elements). The vectorial shape functions for these spaces use appropriate constant vector fields based on the geometry of the master elements, which are multiplied by an available set of H^1 hierarchical scalar shape functions of any degree k . There are two types of shape functions in this methodology. There are those ones of interior type, with vanishing normal components over all element faces. Otherwise, they are classified as of face type, having normal component on the face associated to them coinciding with the restriction of the corresponding scalar shape function used in their definition, and vanishing over the other faces. Then, the shape functions are mapped to the geometrical elements by the Piola transformation, and assembled in order to get continuous normal components.

Following the developments in (Castro et al., 2016) for affine elements, we shall consider for the curved meshes two stable configuration cases for approximation spaces to produce different orders of accuracy for the primal variable ($k + 1$ or $k + 2$), while keeping fixed the order of accuracy ($k + 1$) of the flux variable. By increasing the degree of polynomials used in the primal approximations, stabilization is obtained by enhancing flux spaces with internal shape functions, while keeping the border fluxes of degree k . In all the cases the choices of approximation spaces are guided by the property that, in the master element, the image of the dual space by the divergence operator coincides with the primal space. Furthermore, using static condensation, the global condensed matrices to be solved have reduced dimension, which is proportional to the dimension of border fluxes of degree.

Implementation is performed in the NeopZ computational platform ¹, which is an open-source object-oriented project providing a comprehensive set of high performance tools for finite element simulations. For verification, a test problem with known analytical solution is adopted, showing the expected convergence rates. In order to illustrate the effect of parallelism and static condensation in CPU time reduction, the flow in a porous media around a cylindrical well is also simulated using a sequence of hp-adaptive meshes.

2 $\mathbf{H}(\text{div})$ -CONFORMING APPROXIMATION SUBSPACES

Let $\Gamma = \{K\}$ be a mesh on a domain $\Omega \subset \mathbb{R}^3$ formed by elements K , without limitation on hanging faces, and let $\mathbf{k} = (k_K)$ be a given polynomial order distribution over the elements. Consider approximation subspaces

$$\mathbf{V}_{\mathbf{k}}^{\Gamma} \subset \mathbf{H}(\text{div}, \Omega) = \{\mathbf{q} \in L^2(\Omega)^2; \nabla \cdot \mathbf{q} \in L^2(\Omega)\},$$

¹<http://github.com/labmec/neopz>

which are piecewise defined as $\mathbf{q}|_K = \mathbf{q}_K \in \mathbf{H}(\text{div}, K)$ over the elements $K \in \Gamma$. In order to be globally included in $\mathbf{H}(\text{div}, \Omega)$, the local pieces should be assembled by keeping continuous normal components across common element faces. The proposed methodology used for the construction of such kind of approximation subspaces follows a sequence of steps described below. We shall be concerned with hexahedral, tetrahedral or prismatic meshes.

1. To each element K , there is a geometric mapping $\mathbf{x} : \hat{K} \rightarrow K$, associating each point $\boldsymbol{\xi} \in \hat{K}$ of the master element \hat{K} to a point $\mathbf{p} = \mathbf{x}(\boldsymbol{\xi}) \in K$. An isomorphism $\mathbb{F} : \hat{\varphi} \rightarrow \varphi$, mapping scalar functions of $H^1(\hat{K})$ to scalar functions of $H^1(K)$, is induced by the geometric mapping. It also induces a contravariant Piola transformation $\mathbb{F}^{div} : \hat{\boldsymbol{\Phi}} \rightarrow \boldsymbol{\Phi}$, an isomorphism mapping vector fields $\hat{\boldsymbol{\Phi}} \in \mathbf{H}(\text{div}, \hat{K})$ to vector fields $\boldsymbol{\Phi} \in \mathbf{H}(\text{div}, K)$, which are defined in geometrical elements K by the formula $\boldsymbol{\Phi} = \mathbb{F}[\frac{1}{\det \mathbf{J}} \mathbf{J} \hat{\boldsymbol{\Phi}}]$, where $\mathbf{J} = \nabla \mathbf{x}$ is the Jacobian of the geometric mapping.
2. Polynomial spaces P_k , and hierarchical bases $B_k^{\hat{K}} = \{\hat{\varphi}\}$ of P_k are provided. For tetrahedra, the polynomials in P_k have total degree k , for hexahedra they have maximum degree k in each coordinate, and for prismatic elements, P_k is formed by polynomials of total degree k in (ξ_0, ξ_1) , and of maximum degree k in ξ_2 .
3. Constant vector fields $\hat{\mathbf{v}}$ are defined over the master element. These fields are classified as being of face or internal type. A field associated to a given face is incident to it, and is connected to one of its basic elements: vertex, edge or itself. The internal fields may be connected to the interior of the master element or to fields tangent to an edge or face.
4. A family of hierarchical vectorial bases $\mathbf{B}_k^{\hat{K}} = \{\hat{\boldsymbol{\Phi}}\}$ is given. The principle in their construction is to multiply a scalar basic function $\hat{\varphi} \in B_k^{\hat{K}}$ by a vector field $\hat{\mathbf{v}}$ in order to get $\hat{\boldsymbol{\Phi}} = \hat{\varphi} \hat{\mathbf{v}}$. There are shape functions of interior type, with vanishing normal components over all element faces. Otherwise, $\hat{\boldsymbol{\Phi}}$ is classified as of face type.
5. For a given degree k_K , a vectorial basis $\mathbf{B}_{k_K}^K = \{\boldsymbol{\Phi}\}$ is defined over K by the Piola transformation $\boldsymbol{\Phi} = \mathbb{F}^{div}(\hat{\boldsymbol{\Phi}})$, where $\hat{\boldsymbol{\Phi}} \in \mathbf{B}_{k_K}^{\hat{K}}$.
6. Construction of approximation subspaces $\mathbf{V}_k^\Gamma \subset \mathbf{H}(\text{div}, \Omega)$ formed by functions $\mathbf{q} \in [L^2(\Omega)]^3$, which are defined piecewise over the elements of Γ by local functions $\mathbf{q}_K = \mathbf{q}|_K \in \text{span } \mathbf{B}_{k_K}^K \subset \mathbf{H}(\text{div}, K)$. They can be assembled to get continuous normal components on the elements interfaces. This property is obtained as a consequence of the particular properties verified by the proposed vectorial shape functions and of the continuity of the scalar shape functions used in their construction.

The next subsections are dedicated to a detailed description of these steps. The case of two-dimensional geometries have already been discussed in (Siqueira et al., 2013) for uniform affine partitions, and in (Devloo et al., 2016) for hp -adaptive affine meshes. A detailed explanation is given in (Castro et al., 2016) for 3D affine elements. Preliminary results in uniform curved meshes in 2D regions or manifolds immersed in \mathbb{R}^3 are presented in (Castro et. al., 2016b). The description here applies to 3D curved hp -adaptive partitions, without constraints in hanging sides, and distribution of polynomial degrees.

2.1 Concepts regarding geometry

We shall assume that there is a transformation $\mathbf{x} : \mathbb{R}^3 \rightarrow \mathbb{R}^3$ mapping a master element \hat{K} onto K . Namely, the tetrahedron, hexahedron and prism master elements are, respectively,

$\hat{K} = \mathcal{T}e$, $\hat{K} = \mathcal{H}$ and $\hat{K} = \mathcal{P}r$ defined by

$$\begin{aligned} \mathcal{T}e &= \{ \boldsymbol{\xi} = (\xi_0, \xi_1, \xi_2); \xi_0 \geq 0, \xi_1 \geq 0, \xi_2 \geq 0, \xi_0 + \xi_1 + \xi_2 \leq 1 \}, \\ \mathcal{H} &= [-1, 1]^3, \quad \mathcal{P}r = \mathcal{T} \times [0, 1]. \end{aligned}$$

where $\mathcal{T} = \{ \boldsymbol{\xi} = (\xi_0, \xi_1); \xi_0 \geq 0, \xi_1 \geq 0, \xi_0 + \xi_1 \leq 1 \}$ is the triangular reference element.

Given an element $K \subset \mathbb{R}^3$, let \mathcal{V} , \mathcal{E} and \mathcal{F} be the sets of the vertices, edges and faces of K , respectively. The basic geometric elements of K are mapped from \hat{K} by the geometric transformation \mathbf{x} . For each face $F \in \mathcal{F}$, let \mathcal{V}_F and \mathcal{E}_F be the sets of vertices and edges of F . Given a vertex $a \in \mathcal{V}$, define \mathcal{F}_a as the set of the faces sharing a . Similarly, \mathcal{F}_l is the set of the faces sharing the edge l . One edge is said to be adjacent to the face F by the vertex $a \in \mathcal{V}_F$ if it is common to the two incident faces over F that share this vertex. Equivalently, given an edge $l \in \mathcal{E}_F$, the face sharing l with F is called adjacent to F by this edge.

2.2 Scalar shape functions

The scalar shape functions $\hat{\varphi}$ considered in the present paper are described in (Devloo et al., 2009). They associated with one of the basic elements of \hat{K} , namely, vertex, edge, face or the volume \hat{K} itself, and are characterized by the following main properties:

- Vertex functions $\hat{\varphi} = \varphi^{\hat{a}}(\boldsymbol{\xi})$: they are traditional Lagrangian first order basis functions such that $\varphi^{\hat{a}}(a) = 1$, and vanish in all vertices different from \hat{a} , and edges and faces not sharing the vertex \hat{a} .
- Edge functions $\hat{\varphi} = \varphi^{\hat{l}, n}(\boldsymbol{\xi})$: they vanish in all edges different from \hat{l} , and in all faces not sharing \hat{l} .
- Face functions $\hat{\varphi} = \varphi^{\hat{F}, n_1, n_2}(\boldsymbol{\xi})$, they vanish in all edges, vertices, and faces other than \hat{F} .
- Internal functions $\hat{\varphi} = \varphi^{\hat{K}, n_1, n_2, n_3}(\boldsymbol{\xi})$: they vanish in all faces, edges and vertices of \hat{K} .

	Vertex	Edge	Face	Internal	Total
$\mathcal{T}e$	4	$6(k-1)$	$\frac{1}{2}(k-1)(k-2)$	$\frac{1}{6}(k-1)(k-2)(k-3)$	$\frac{1}{6}(k+1)(k+2)(k+3)$
\mathcal{H}	8	$12(k-1)$	$6(k-1)^2$	$(k-1)^3$	$(k+1)^3$
$\mathcal{P}r$	6	$9(k-1)$	$(k-1)(4k-5)$	$\frac{1}{2}(k-1)^2(k-2)$	$\frac{1}{2}(k+1)^2(k+2)$

Table 1: Number of scalar shape functions in $B_k^{\hat{K}}$.

The shape functions associated with edge, face and volume elements are formed by the product of two functions. The first one, called blending function, is a specific combination of vertex functions. There is one blending function for each basic element, and its role is to enforce the corresponding vanishing property on the other elements. In order to increase the degrees of the shape functions, the blending functions are multiplied by a second function formed by the product of Chebyshev polynomials (of degree n or n_i), which vary according to particular geometry. These Chebyshev polynomials are evaluated in parameters determined by appropriate affine transformations of the master element coordinates.

The resulting set of functions

$$\mathcal{B}_k^{\hat{K}} = \left\{ \varphi^{\hat{a}}, \varphi^{\hat{l}_m, n}, \varphi^{\hat{F}, n_1, n_2}, \varphi^{\hat{K}, n_1, n_2, n_3} \right\}$$

is linearly independent, spanning a subspace of $H^1(\hat{K})$. The total numbers of each type of shape functions in $\mathcal{B}_k^{\hat{K}}$ are indicated in Table 1.

2.3 Vector fields

Connected to each basic geometric element of \hat{K} (vertex, edge, face, or volume), three linearly independent constant vector fields are defined by the following instructions:

- For each vertex \hat{a} , there are three fields $\mathbf{v} = \mathbf{v}^{\hat{F}, \hat{a}}$, each one associated with a face \hat{F} having \hat{a} as one of its vertices. The vector $\mathbf{v}^{\hat{F}, \hat{a}}$ should be aligned to the edge adjacent to \hat{F} by the vertex \hat{a} . Furthermore, it is normalized to have unit normal component over \hat{F} .
- For each edge \hat{l} , there is a vector $\mathbf{v} = \mathbf{v}^{\hat{l}, \top}$, aligned to \hat{l} , and there are two vectors $\mathbf{v} = \mathbf{v}^{\hat{F}, \hat{l}}$, which are incident to \hat{F} and parallel to the face adjacent to \hat{F} by \hat{l} . They are normalized to have unit normal component over \hat{F} .
- For each face \hat{F} , there is the outward unit normal $\mathbf{v} = \mathbf{v}^{\hat{F}, \perp}$ and two linearly independent vectors $\mathbf{v} = \mathbf{v}_{(j)}^{\hat{F}, \top}$, $j = 1, 2$ tangent to \hat{F} .
- Associated with the volume \hat{K} itself, there are orthonormal vector fields $\mathbf{v} = \mathbf{v}_{(j)}^{\hat{K}} = \mathbf{e}_{(j)}$, $j = 1, 2, 3$ associated with it. For instance, they can be defined by the canonical orthonormal vectors $e_{(1)} = (1, 0, 0)$, $e_{(2)} = (0, 1, 0)$ and $e_{(3)} = (0, 0, 1)$.

The vector fields are grouped into two categories:

1. Face vector fields, which are incident to the faces \hat{F} :
 - a) $\mathbf{v} = \mathbf{v}^{\hat{F}, \hat{a}}$, vectors associated with the vertices \hat{a} of \hat{F} .
 - b) $\mathbf{v} = \mathbf{v}^{\hat{F}, \hat{l}}$ vectors associated with the edges \hat{l} of \hat{F} .
 - c) $\mathbf{v} = \mathbf{v}^{\hat{F}, \perp}$ vector associated (normal) with the face \hat{F} itself.
2. Internal vector fields
 - a) $\mathbf{v} = \mathbf{v}^{\hat{l}, \top}$, vector aligned to the edges \hat{l} ,
 - b) $\mathbf{v} = \mathbf{v}_{(j)}^{\hat{F}, \top}$, $j = 1, 2$, vectors tangent to the faces \hat{F} .
 - c) $\mathbf{v} = \mathbf{v}_{(j)}^{\hat{K}} = \mathbf{e}_{(j)}$, $j = 1, 2$ and 3 , associated with the volume \hat{K} .

2.4 Vectorial basis functions in $\mathbf{H}(\text{div}, \hat{K})$

The purpose is to construct vectorial bases $\mathbf{B}_k^{\hat{K}}$ formed by functions $\hat{\Phi} \in \mathbf{H}(\text{div}, \hat{K})$ defined on the element \hat{K} by the multiplication

$$\hat{\Phi} = \hat{\varphi} \mathbf{v},$$

where \mathbf{v} is one of the constant vector fields defined in Section 2.3, and $\hat{\varphi}$ is one of the scalar basis functions in $\mathcal{B}_k^{\hat{K}}$, described in Section 2.2. It is clear that $\nabla \cdot \hat{\Phi} = \mathbf{v} \cdot \nabla \hat{\varphi}$, which implies that $\hat{\Phi} \in \mathbf{H}(\text{div}, \hat{K})$. These vectorial shape functions shall be classified as face or internal functions, verifying the following properties.

Face functions:

- The face functions $\Phi^{\hat{F},\hat{a}} = \varphi^{\hat{a}} \mathbf{v}^{\hat{F},\hat{a}}$: they vanish on the face that do not have \hat{a} as one of its vertices because the scalar functions $\varphi^{\hat{a}}$ verify this property. If \hat{a} is a vertex of another face adjacent \hat{F} by \hat{a} , then the normal component of $\Phi^{\hat{F},\hat{a}}$ restricted to it also vanishes, because $\mathbf{v}^{\hat{F},\hat{a}}$ is parallel to this adjacent face. The normal component $\Phi^{\hat{F},\hat{a}} \cdot \mathbf{n}^{\hat{K}}|_{\hat{F}} = \varphi^{\hat{a}}|_{\hat{F}}$, having in mind that the normal component of $\mathbf{v}^{\hat{F},\hat{a}}$ is unitary over \hat{F} .
- The face functions $\Phi^{\hat{F},\hat{l},n} = \varphi^{\hat{l},n} \mathbf{v}^{\hat{F},\hat{l}}$: they vanish on the faces that do not have \hat{l} as one of its edges because the scalar functions $\varphi^{\hat{l},n}$ verify this property. Otherwise, the normal component of $\Phi^{\hat{F},\hat{l},n}$ restricted to a face adjacent to \hat{F} by \hat{l} vanishes, because $\mathbf{v}^{\hat{F},\hat{l}}$ is parallel to it. Having in mind that the normal component of $\mathbf{v}^{\hat{F},\hat{l}}$ is unitary over \hat{F} , it follows that $\Phi^{\hat{F},\hat{l},n} \cdot \mathbf{n}^{\hat{K}}|_{\hat{F}} = \varphi^{\hat{l},n}|_{\hat{F}}$,
- The face functions $\Phi^{\hat{F},n_1,n_2} = \varphi^{\hat{F},n_1,n_2} \mathbf{v}^{\hat{F},\perp}$: they vanish on the faces different from \hat{F} , because the scalar functions $\varphi^{\hat{F},n}$ have this property. Over \hat{F} , the normal component $\Phi^{\hat{F},n} \cdot \mathbf{n}^{\hat{K}}|_{\hat{F}} = \varphi^{\hat{F},n_1,n_2}|_{\hat{F}}$, having in mind that $\mathbf{v}^{\hat{F},\perp}$ coincides with the outward unit normal to \hat{F} .

Internal functions:

- The internal functions $\Phi^{\hat{K},\hat{l},n} = \varphi^{\hat{l},n} \mathbf{v}^{\hat{l},\top}$: they vanish on all faces not sharing \hat{l} , since the scalar function $\varphi^{\hat{l},n}$ satisfy this property. Otherwise, the normal component of $\Phi^{\hat{K},\hat{l},n}$ restricted to a face sharing \hat{l} also vanishes, having in mind that $\mathbf{v}^{\hat{l},\top}$ is tangent to it.
- The internal functions $\Phi_{(j)}^{\hat{K},n_1,n_2,n_3} = \varphi^{\hat{K},n_1,n_2,n_3} \mathbf{v}_{(j)}^{\hat{K}}$: they vanish on all faces, since the internal functions $\varphi^{\hat{K},n_1,n_2,n_3}$ verify this property.

Let $\mathbf{B}_k^{\hat{K}}$ be the set formed by these face and internal vectorial shape functions

$$\mathbf{B}_k^{\hat{K}} = \underbrace{\left\{ \Phi^{\hat{F},\hat{a}}, \Phi^{\hat{F},\hat{l},n}, \Phi^{\hat{F},n_1,n_2} \right\}}_{\text{face functions}} \cup \underbrace{\left\{ \Phi^{\hat{K},\hat{l},n}, \Phi_{(1)}^{\hat{K},\hat{F},n_1,n_2}, \Phi_{(2)}^{\hat{K},\hat{F},n_1,n_2}, \Phi_{(1)}^{\hat{K},n_1,n_2,n_3}, \Phi_{(2)}^{\hat{K},n_1,n_2,n_3}, \Phi_{(3)}^{\hat{K},n_1,n_2,n_3} \right\}}_{\text{internal functions}}.$$

It is linearly independent, and span $\mathbf{B}_k^{\hat{K}} \subset \mathbf{H}(\text{div}, \hat{K})$.

2.5 Piola transformation $\Phi = \mathbb{F}^{div} \hat{\Phi}$

Let $\mathbf{x} : \hat{K} \rightarrow K$ be a regular geometric mapping. The scalar functions defined in the master element \hat{K} may be mapped to functions defined in K by the operator $\varphi = \mathbb{F}\hat{\varphi}$ defined by the composition

$$\varphi = \hat{\varphi} \circ \mathbf{x}^{-1}.$$

In building a subspace of $\mathbf{H}(\text{div}, K)$ by the transformation of vector fields in $\mathbf{H}(\text{div}, \hat{K})$, the operator \mathbb{F} does not apply, since it can not preserve normal components, not even mapping $\mathbf{H}(\text{div}, \hat{K})$ on $\mathbf{H}(\text{div}, K)$. For this, the contravariant Piola transformation $\mathbb{F}^{div} : \hat{\Phi} \rightarrow \Phi$,

associated with the geometric mapping \mathbf{x} , is used to relate vectorial functions $\hat{\Phi}$ defined in the master element \hat{K} with vectorial functions Φ defined in geometrical elements K by the formula

$$\Phi = \mathbb{F}\left[\frac{1}{\det \mathbf{J}} \mathbf{J} \hat{\Phi}\right]. \quad (1)$$

As reported in (Brezzi & Fortin, 1991), divergence of vectorial functions given by the Piola contravariant transformation verifies the expression

$$\nabla \cdot \Phi = \mathbb{F}\left[\frac{1}{\det \mathbf{J}} \hat{\nabla} \cdot \hat{\Phi}\right]. \quad (2)$$

Furthermore, if $\varphi = \mathbb{F}\hat{\varphi}$, the following identities are valid

$$\begin{aligned} \int_K \Phi \cdot \nabla \varphi \, d\mathbf{p} &= \int_{\hat{K}} \hat{\Phi} \cdot \hat{\nabla} \hat{\varphi} \, d\xi, \\ \int_K \varphi \nabla \cdot \Phi \, d\mathbf{p} &= \int_{\hat{K}} \hat{\varphi} \hat{\nabla} \cdot \hat{\Phi} \, d\xi, \\ \int_{\partial K} \Phi \cdot \mathbf{n} \varphi \, d\sigma &= \int_{\partial \hat{K}} \hat{\Phi} \cdot \hat{\mathbf{n}} \hat{\varphi} \, d\hat{\sigma}. \end{aligned}$$

As a result, \mathbb{F}^{div} is an isomorphism between $\mathbf{H}(\text{div}, \hat{K})$ and $\mathbf{H}(\text{div}, K)$, preserving normal components, in the $H^{-1/2}$ sense.

2.6 Approximation spaces in $\mathbf{H}(\text{div}, \Omega)$

As stated in the beginning of this section, the construction of vectorial shape functions $\Phi \in \mathbf{H}(\text{div}, K)$ to form a basis $\mathbf{B}_{k_K}^K$ on the curved element K , starts with shape functions of type $\hat{\Phi} = \hat{\varphi} \hat{\mathbf{v}}$ in $\mathbf{B}_{\hat{k}}^{\hat{K}}$, defined in the master element. The next step is the application of Piola transformation $\Phi = \mathbb{F}^{div} \hat{\Phi}$ to obtain

$$\begin{aligned} \Phi &= \mathbb{F}\left[\frac{1}{\det \mathbf{J}} \mathbf{J} \hat{\Phi}\right] \\ &= \mathbb{F}\left[\hat{\varphi} \frac{1}{\det \mathbf{J}} \mathbf{J} \hat{\mathbf{v}}\right] = \varphi \mathbf{b}, \end{aligned}$$

where $\varphi = \mathbb{F}\hat{\varphi}$, and $\mathbf{b} = \mathbb{F}\left[\frac{1}{\det \mathbf{J}} \mathbf{J} \hat{\mathbf{v}}\right] = \mathbb{F}^{div} \hat{\mathbf{v}}$. Let \mathbf{B}_k^K be the set formed by edge and internal functions obtained by this construction procedure

$$\begin{aligned} \mathbf{B}_k^K &= \underbrace{\{\Phi^{F,a}, \Phi^{F,l,n}, \Phi^{F,n_1,n_2}\}}_{\text{face functions}} \\ &\cup \underbrace{\{\Phi^{K,l,n}, \Phi_{(1)}^{K,F,n_1,n_2}, \Phi_{(2)}^{K,F,n_1,n_2}, \Phi_{(1)}^{K,n_1,n_2,n_3}, \Phi_{(2)}^{K,n_1,n_2,n_3}, \Phi_{(3)}^{K,n_1,n_2,n_3}\}}_{\text{internal functions}}. \end{aligned}$$

By the property (1), it follows that $\text{span } \mathbf{B}_k^K \subset \mathbf{H}(\text{div}, K)$.

Let $\Gamma = \{K\}$ be a mesh formed by elements K with any of \mathcal{T}_e , \mathcal{H} or \mathcal{P}_r geometries. Furthermore, we assume no limitation on hanging faces, and on polynomial order distribution $\mathbf{k} = (k_K)$ over the elements. Our purpose is to construct approximation subspaces $\mathbf{V}_{\mathbf{k}}^\Gamma \subset$

$\mathbf{H}(\text{div}, \Omega)$ formed by functions \mathbf{q} piecewise defined over the elements of Γ by local functions $\mathbf{q}_K = \mathbf{q}|_K \in \text{span } \mathbf{B}_{k_K}^K$. In order to be a function in $\mathbf{H}(\text{div}, \Omega)$, the normal components of \mathbf{q} across the interfaces $F = K^\ell \cap K^j$ between two neighbouring elements K^ℓ and K^j should be continuous. This means that the jump on the normal component of \mathbf{q} across F

$$[\mathbf{q}^{K^\ell} \cdot \mathbf{n}^{K^j} + \mathbf{q}^{K^j} \cdot \mathbf{n}^{K^\ell}]_F$$

should vanish. As described next, this property is obtained as a consequence of the particular properties verified by the proposed vectorial shape functions and of the continuity of the scalar shape functions across the interfaces used in their construction.

Since the contravariant Piola transformation preserves zero normal components, mapping tangent vectors in \hat{F} to tangent vectors in $F = \mathbf{x}\hat{F}$, then the non-zero contributions to the normal component of \mathbf{q}^{K^ℓ} on the face F come from the face functions $\Phi^{F,a}$, $\Phi^{F,l,n}$ and Φ^{F,n_1,n_2} associated with its vertices, edges and to the face F itself. Precisely,

$$\begin{aligned} \mathbf{q}^{K^\ell} \cdot \mathbf{n}^{K^\ell}|_F &= \left[\sum_{a \in \mathcal{V}_F} \alpha_{F,a} \varphi^a \mathbf{b}^{F,a} \cdot \mathbf{n}^{K^\ell} + \sum_{l \in \mathcal{E}_F} \sum_n \beta_{F,l,n} \varphi^{l,n} \mathbf{b}^{F,l,n} \cdot \mathbf{n}^{K^\ell} \right. \\ &\quad \left. + \sum_{n_1, n_2} \gamma_{F,n_1, n_2} \varphi^{F,n_1, n_2} \mathbf{b}^{F,n_1, n_2} \cdot \mathbf{n}^{K^\ell} \right]_F. \end{aligned}$$

In (Castro, 2016b), a procedure was described for creating vector functions which have unit normal components over the element interface. In that context, assuming the continuity of the scalar basis functions across the interface F , and recalling that $\mathbf{n}^{K^j} = -\mathbf{n}^{K^\ell}$, the jump on the normal component of \mathbf{q} over F vanishes if and only if in the expansions of \mathbf{q}^{K^ℓ} and \mathbf{q}^{K^j} the sum of the two coefficients multiplying each of the face functions associated with the vertices, edges and face of the interface F is zero. However, the vector functions used in this contribution differ from the functions define in (Castro et al., 2016b) by the determinant of the Jacobian associated with the interface and therefore ensures continuity of the normal component as well. The procedure to ensure continuity of the scalar basis based on hp -adaptive meshes is described in (Calle et al., 2015). The combination of the continuity of the scalar shape functions and vector functions ensures the continuity of the normal component of the shape functions.

3 Application to mixed finite element formulations

We consider the classical mixed formulation for the elliptic Poisson problem

$$\nabla \cdot \boldsymbol{\sigma} = f \text{ in } \Omega, \quad (3)$$

$$\boldsymbol{\sigma} = -\nabla u \text{ in } \Omega, \quad (4)$$

$$u = u_D \text{ on } \partial\Omega_D, \quad (5)$$

$$\nabla u \cdot \boldsymbol{\eta} = g \text{ on } \partial\Omega_N. \quad (6)$$

As studied in (Brezzi & Fortin, 1991), the variational mixed formulation of problem (4)-(6) is: find $u \in L^2(\Omega)$ and $\boldsymbol{\sigma} \in H\text{div}(\Omega)$, with $\boldsymbol{\sigma} = \boldsymbol{\sigma}_N$ on $\partial\Omega_N$, such that

$$\int_{\Omega} \boldsymbol{\sigma} \cdot \mathbf{q} \, d\Omega - \int_{\Omega} u \nabla \cdot \mathbf{q} \, d\Omega = - \int_{\partial\Omega_D} u_D \mathbf{q} \cdot \boldsymbol{\eta} \, ds, \quad (7)$$

$$\int_{\Omega} \nabla \cdot \boldsymbol{\eta} \, v \, d\Omega = \int_{\Omega} f v \, d\Omega, \quad (8)$$

for all $\mathbf{q} \in \mathbf{H}div(\Omega)$, with $\mathbf{q} \cdot \boldsymbol{\eta}|_{\partial\Omega_N} = 0$, and $v \in L^2(\Omega)$.

The purpose is to solve this kind of problem using discrete versions of mixed formulation based finite element approximation spaces $\mathbf{V}^\Gamma \subset \mathbf{H}(div, \Omega)$ for $\boldsymbol{\sigma}$, and $U^\Gamma \subset L^2(\Omega)$ for u . These spaces are based on curved meshes Γ , which can be non-conformal. Precisely, the functions u in U^Γ and \mathbf{q} in \mathbf{V}^Γ are piecewise defined as $u|_K = \mathbb{F}_K \hat{u}$, and $\mathbf{q}|_K = \mathbb{F}_K^{div} \hat{\mathbf{q}}$, in terms of functions $\hat{u} \in U^{\hat{K}}$, $\hat{\mathbf{q}} \in \mathbf{V}^{\hat{K}}$ defined in polynomial approximation spaces $(\mathbf{V}^{\hat{K}}, U^{\hat{K}})$ on the master element, which can have non-uniform degree distribution over the elements K . However, it is well known that they should be consistent in order to produce stable approximations. In this sense, the effect of the exact deRham property

$$\nabla \cdot \mathbf{V}^{\hat{K}} = U^{\hat{K}} \quad (9)$$

on the stability of the discrete mixed problem is crucial. Two cases for the choice of approximation space configuration $(\mathbf{V}^\Gamma, U^\Gamma)$ shall be considered for all element geometries.

Approximation spaces of type $\mathbf{P}_k^* P_k$. The flux approximations in $\mathbf{V}^\Gamma \subset \mathbf{H}(div, \Omega)$ are said to be of \mathbf{P}_k^* type if, for each element K in the partition Γ , the corresponding polynomial spaces $\mathbf{V}^{\hat{K}}$ in the master element is spanned by the face functions of \mathbf{P}_{k_K} type, and by the internal shape functions of \mathbf{P}_{k_K+1} defined by vectorial polynomials of degree $k_K + 1$ whose divergence are included in the scalar approximation space $U^{\hat{K}}$ of type P_{k_K} . Since the incomplete flux approximation space of type \mathbf{P}_k^* only involves the complete vector valued polynomials of degree \mathbf{k} , in simulations using $\mathbf{P}_k^* P_k$ configurations with uniform mesh spacing $h_K = h$ and polynomial degree distributions $k_K = k, \forall K$, the expected L^2 -error convergence rates are of order $k + 1$ for both $\boldsymbol{\sigma}$ and u variables. This is the type of RT_k space configuration for rectangular (Raviat & Thomas, 1977) and hexahedral geometries (Nédélec, 1980), and of $BDFM_{k+1}$ elements for triangular (Brezzi et al., 1987) and tetrahedral elements (Brezzi & Fortin, 1991).

Approximation spaces of type $\mathbf{P}_k^{} P_{k+1}$.** This is a new space configuration introduced in (Castro et al., 2016a) for affine meshes. The idea for the construction of flux approximation spaces of type \mathbf{P}_k^{**} consists in adding to the complete vector valued spaces of type \mathbf{P}_k those interior shape functions of $\mathbf{P}_{k_K+1}^*$ defined in the master element by vectorial polynomials of degree $\mathbf{k}_K + 2$ whose divergence are included in the scalar approximation space of type P_{k_K+1} . Therefore, in \mathbf{P}_k^{**} the face shape functions are still obtained from polynomials of degree $\leq k_K$, but some of the internal shape functions may be obtained from polynomials of degree up to $k_K + 2$. As in the previous case, here the verification of property (9) is the basic principle guiding the definition of the pair of approximation spaces. In simulations using $\mathbf{P}_k^{**} P_{k+1}$ configurations with uniform mesh spacing $h_K = h$ and polynomial degree distributions $k_K = k, \forall K$, and since the spaces of type \mathbf{P}_k^{**} only involves the complete vector valued polynomials of degree \mathbf{k} , the L^2 -error convergence rate of order $k + 1$ is expected for the flux variable. However, for the variable u a higher order $k + 2$ of convergence may be reached.

4 Numerical experiments

In this section, numerical experiments are performed for the evaluation of convergence and computational efficiency of two different approximation space configurations $\mathbf{P}_k^* P_k$ and

$\mathbf{P}_k^{**} P_{k+1}$ to the mixed formulation when applied to curved meshes. In plots of the numerical results, these mixed methods will be referred by the acronyms MF^* or MF^{**} , respectively. They are applied to two test problems: one is defined in a spherical region with a hollow in the middle having a known smooth solution. The second one is meant to simulate a flow in a porous media represented by oval region around a horizontal well. The solution is expected presents strong gradients in the vicinity of the well toe and heel.

The discrete mixed formulations are implemented using static condensation techniques using the following organization of the degrees of freedom. The degrees of freedom of the flux may be organized in the form σ_i, σ_e , where σ_i and σ_e refer to internal and edge components of the flux, respectively. For the variable u , let u_0 be a scalar value and u_i denote the remaining degrees of freedom except u_0 . Thus, the matrix representation of the discrete mixed formulation can be expressed in the form

$$\begin{pmatrix} A_{ii} & B_{ii}^T & B_{ie}^T & A_{ie} \\ B_{ii} & 0 & 0 & B_{ie} \\ B_{ie} & 0 & 0 & B_{ee} \\ A_{ei} & B_{ie}^T & B_{ee}^T & A_{ee} \end{pmatrix} \begin{pmatrix} \sigma_i \\ u_i \\ u_0 \\ \sigma_e \end{pmatrix} = \begin{pmatrix} -u_D \\ -f_i \\ -f_0 \\ 0 \end{pmatrix}.$$

Then, static condensation may be applied by eliminating the internal degrees of freedom σ_i and u_i , to get a condensed system in terms of σ_e and u_0 .

It should be observed that, for each kind of element geometry, the dimension of the static condensed matrix is determined by the number of degrees of freedom of the face components plus one, which coincides for both approximations spaces of types $\mathbf{P}_k^* P_k$ and $\mathbf{P}_k^{**} P_{k+1}$.

4.1 Problem 1: smooth solution

In this example, the domain $\Omega = \{\mathbf{x} \in \mathbb{R}^3; \frac{1}{4} \leq \|\mathbf{x}\| \leq 1\}$, and the analytic solution is given by the formula

$$u = \frac{\pi}{2} - \tan^{-1} \left(d \left(\sqrt{(x-a)^2 + (y-b)^2 + (z-c)^2} - \frac{\pi}{3} \right) \right)$$

$$\sigma = -\nabla u = \begin{cases} \frac{d(x-a)}{\sqrt{(a-x)^2 + (b-y)^2 + (c-z)^2} \left(d^2 \left(\sqrt{(a-x)^2 + (b-y)^2 + (c-z)^2} - \frac{\pi}{3} \right)^2 + 1 \right)} \\ \frac{d(y-b)}{\sqrt{(a-x)^2 + (b-y)^2 + (c-z)^2} \left(d^2 \left(\sqrt{(a-x)^2 + (b-y)^2 + (c-z)^2} - \frac{\pi}{3} \right)^2 + 1 \right)} \\ \frac{d(z-c)}{\sqrt{(a-x)^2 + (b-y)^2 + (c-z)^2} \left(d^2 \left(\sqrt{(a-x)^2 + (b-y)^2 + (c-z)^2} - \frac{\pi}{3} \right)^2 + 1 \right)} \end{cases}$$

where the coefficients are $a = \frac{5}{4}$, $b = c = -\frac{1}{4}$, and $d = 5$. Dirichlet boundary conditions are enforced in $\partial\Omega_D = \partial\Omega$.

For this problem, regular meshes $\Gamma = \Gamma_h$ formed by curved tetrahedral and hexahedral elements are used. The curved hexahedral meshes are obtained by a projection of uniform square meshes on the faces of a cube, with spacing $h = 2^{-i}$, $i = 0, 1, \dots, 4$, onto the internal

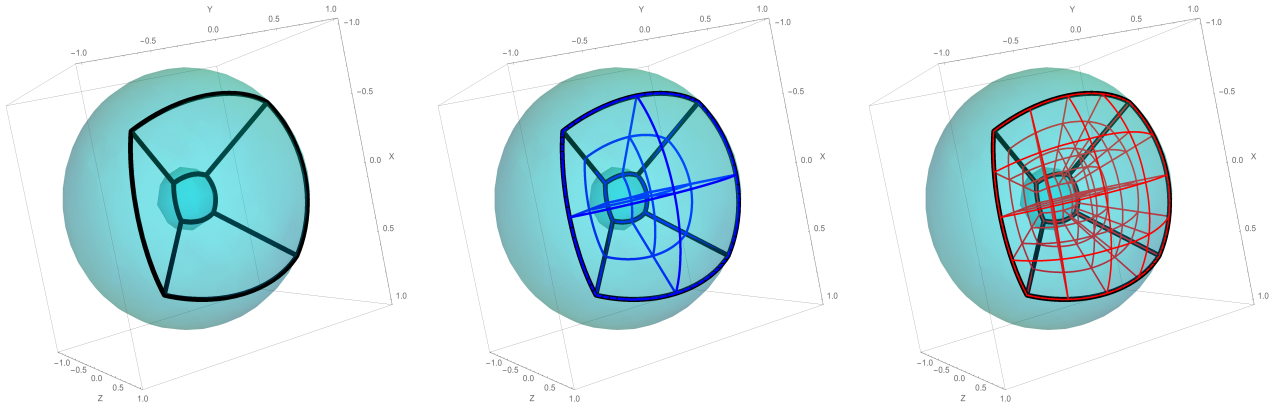


Figure 1: Illustration of curved hexahedral elements of the spherical region in Problem 1: black lines indicate the edges of one curved element at the coarsest level; blue and red curves refer to the next two subsequent refinements, respectively.

and external spherical surfaces of radius $\frac{1}{4}$ and 1. Then, these two surface curved quadrilateral meshes are *blended* (see (Lucci, 2009)) to form a grid on the entire 3D region Ω by transfinite interpolation. In Fig. 1 this process is illustrated for one element at the coarsest level (left side) and its two subsequent refinements. The tetrahedral meshes are obtained from curved prismatic elements, with curved triangular faces over spherical surfaces uniformly sampled at radii $\frac{1}{4} + \frac{3}{4}2^{-j}$. The edges of the triangular spherical surfaces are obtained by quadratic interpolation. Each of these prismatic elements are subdivided into 3 tetrahedral elements to form a tetrahedral mesh for the domain Ω .

For the resolution of the condensed systems, a direct frontal linear solver is used, which has been performed on a Mac Pro desktop computer having the following basic configuration: 2×2.03 GHz 6-Core Intel Xeon Processor, and 64 GB 1333 MHz DDR3 ECC of memory.

Figure 2 presents L^2 -error curves for u and for the flux $\sigma = -\nabla u$ obtained with the two space configurations under consideration for mixed method, for uniform degree distribution $k = 1, 2, 3$ and 4. For the MF^* configuration in hexahedral and tetrahedral meshes, corresponding to the classic RT_k and $BDMF_{k+1}$ spaces, u and the flux are approximated with accuracy of order $k + 1$. For the new case MF^{**} , the flux is approximated with accuracy of order $k + 1$, but enhanced order $k + 2$ is verified for the variable u in both geometries.

Figure 3 illustrates the effectiveness of the static condensation procedure in the reduction of degrees of freedom at the finest level of refinement. More degrees of freedom can be condensed when increasing the polynomial order. Hexahedral elements have a larger number of *condensable* degrees of freedom. For instance, for $k = 4$, and using the $\mathbf{P}_k^* P_k$ space configuration, about 87% of the total number of degrees of freedom is condensed using hexahedral elements, and about 81% for tetrahedral elements. Using the $\mathbf{P}_k^{**} P_{k+1}$ space configuration, about 92% of the total number of degrees of freedom is condensed using hexahedral elements, and about 87% for tetrahedral elements. Since both space configurations share the same face shape functions, but the $\mathbf{P}_k^{**} P_{k+1}$ case uses more internal flux shape functions and scalar shape functions with degree augmented by one, the effect of static condensation is more significant for this richer space configuration.

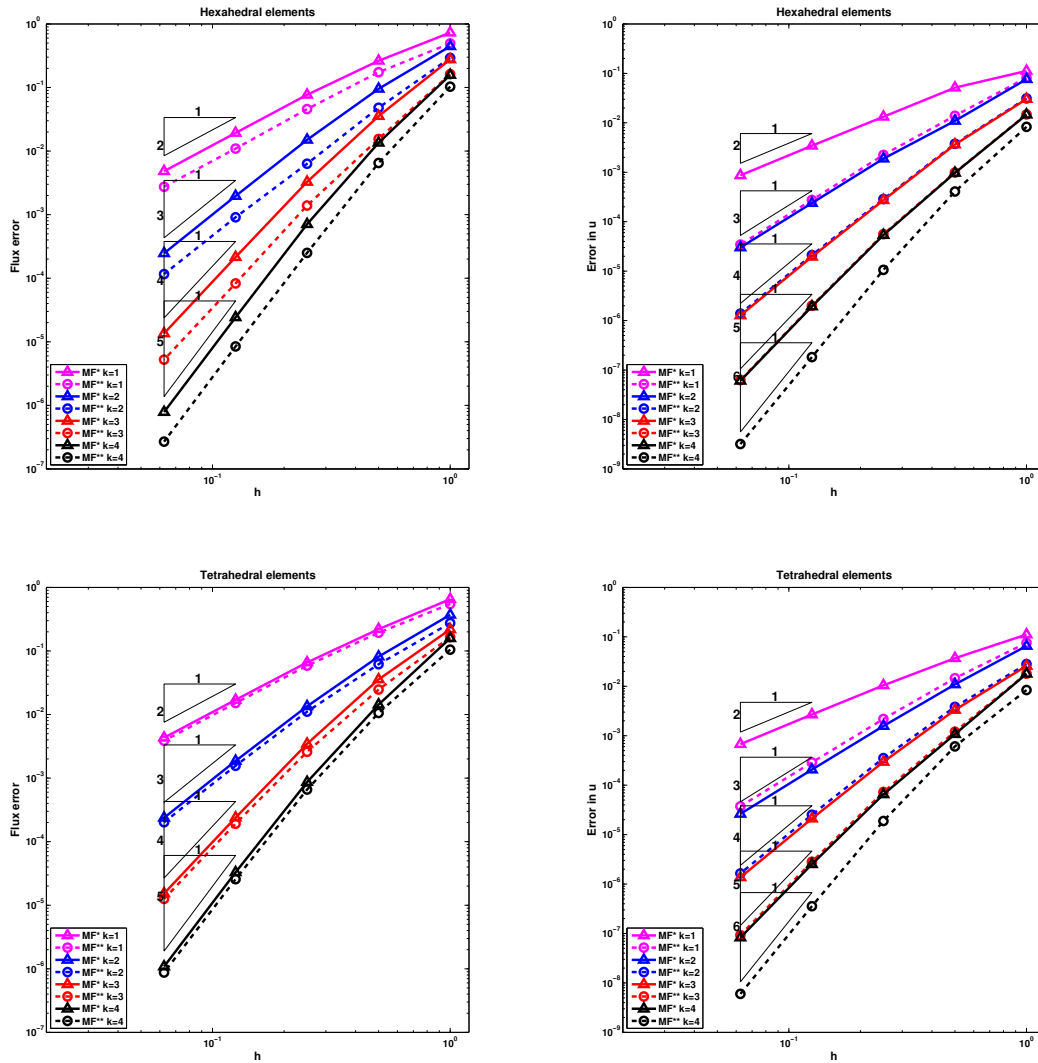


Figure 2: Problem 1: L^2 -error curves in terms of h for ∇u (left side) and for u (right side), using the mixed formulations with $P_k^*P_k$ and $P_k^{**}P_{k1}$ space configurations based on curved hexahedral (top side) and tetrahedral (bottom side) uniform meshes, for $k = 1, 2, 3$ and 4.

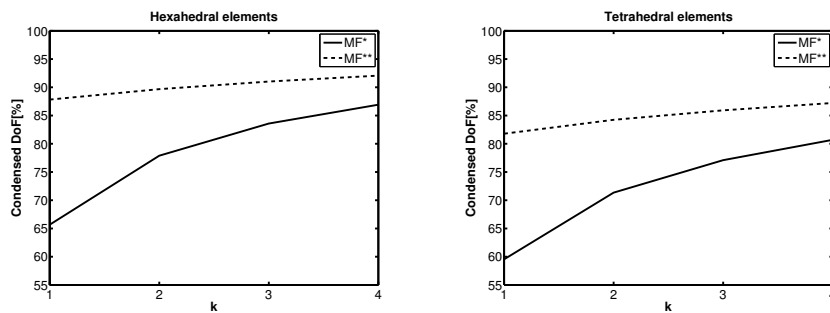


Figure 3: Problem 1: percentage of condensed degrees of freedom in the discrete mixed method using $P_k^*P_k$ and $P_k^{**}P_{k1}$ space configurations at the finest refinement level of hexahedral (left side) and tetrahedral (right side) meshes.

4.2 Problem 2: fluid flow in a porous media around a horizontal well

The purpose of this problem is to simulate the flow around a horizontal well with elliptical drainage area. Dirichlet boundary conditions for the pressure $u = 1$ are applied on the outer elliptical belt, and $u = 0$ on the well, and no flow on the top and bottom of the region are enforced. The source term is $f = 0$.

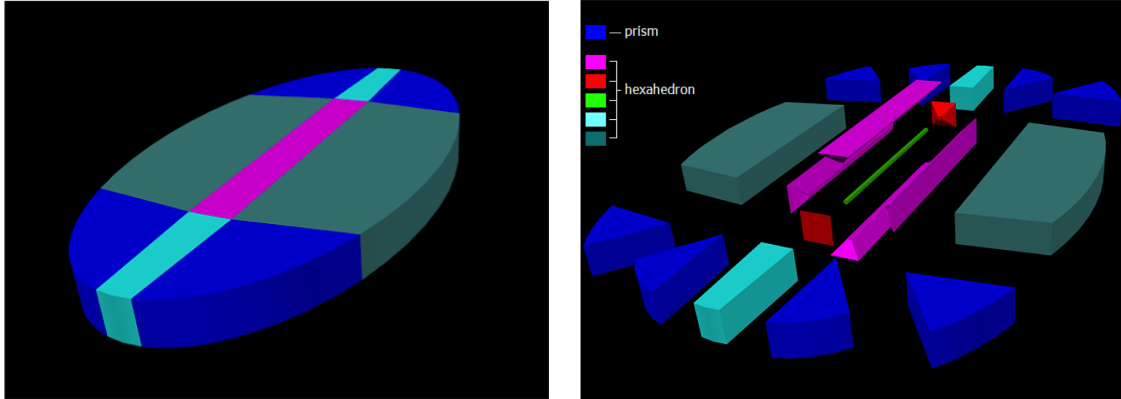


Figure 4: Problem 2: initial mesh (left side) and its details (right side).

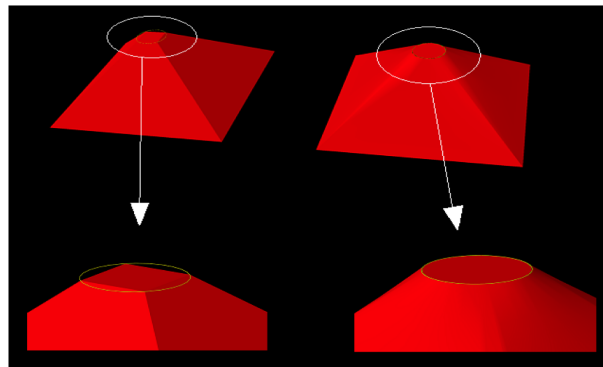


Figure 5: Problem 2: transfinite hexahedron matching the circular well.

The steps for the construction of the adaptive meshes are:

1. Initial mesh composed of transfinite elements: 11 hexahedra and 8 prisms as indicated in Fig. 4. The transfinite mesh interpolation in order to match the hexahedral elements to the circular well is illustrated in Fig. 5.
2. Directional mesh refinement towards the well, and transversal refinement along the well are applied, as illustrated in Fig. 6 (left side).
3. A basic polynomial degree k is applied all over the mesh. Fixing uniform polynomial degree $k_{max} > k$ for the elements touching the toe and heel circular rings, the neighboring elements are assigned one degree lower. The procedure is repeated until the neighboring elements have order k (see Fig. 6 (right side)).

The simulations for this second problem have been performed on a MacBook computer having 4 processors and 8GB of memory. Matrix computation and assembly used Pthreads and

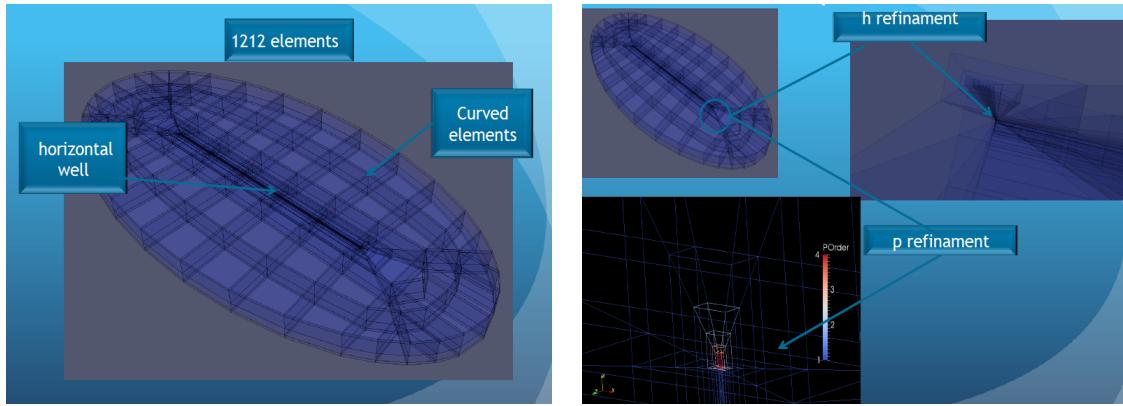


Figure 6: Problem 2: curved mesh geometry after refinement (left side) and illustration of the hp -refinement close to the well toe (right side).

direct skyline algorithm is adopted as linear solver. Meshes are considered with the following parameters: $k = 1$, $k = 2$ or $k = 3$, and 8 or 12 transversal element subdivisions along the well.

In Fig. 7 plots of the flux for the different mesh configurations. It can be observed the singular behaviour of this quantity at well toe and heel, fact that motivates the use of hp -adaptivity procedure in order to resolve it properly. Figure 8 (left side) shows the productivity index obtained with different mesh configurations, confirming a convergence tendency after mesh refinements. The effect of combining static condensation and paralellization is illustrated in Fig. 8 (right side). Using these techniques for the simulation with a mesh configuration where $k = 2$ in the far field, $k_{max} = 5$, and 12 elements are used at the well, the CPU time is about 8% of the required CPU time without using them.

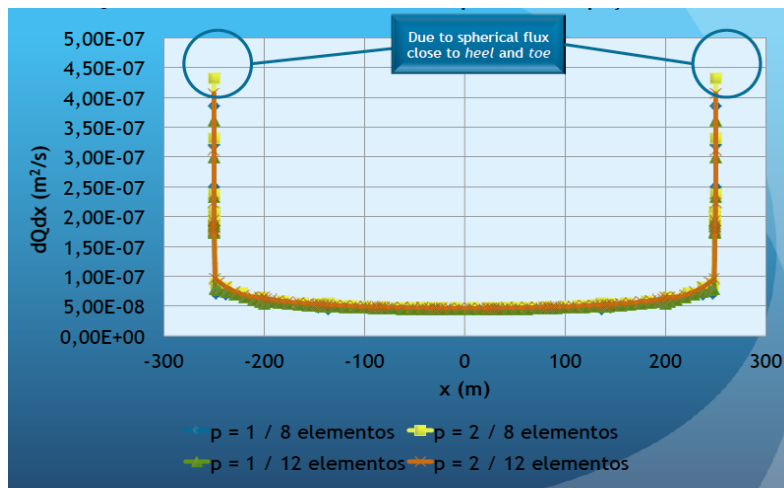


Figure 7: Problem 2: singular flux behaviour close to well heel and toe.

ACKNOWLEDGEMENTS

The authors thankfully acknowledge financial support from CNPq - the Brazilian Research Council (grants 310369/2006-1, 308632/2006-0, 305425/2013-7 and 233323/2014-7). This

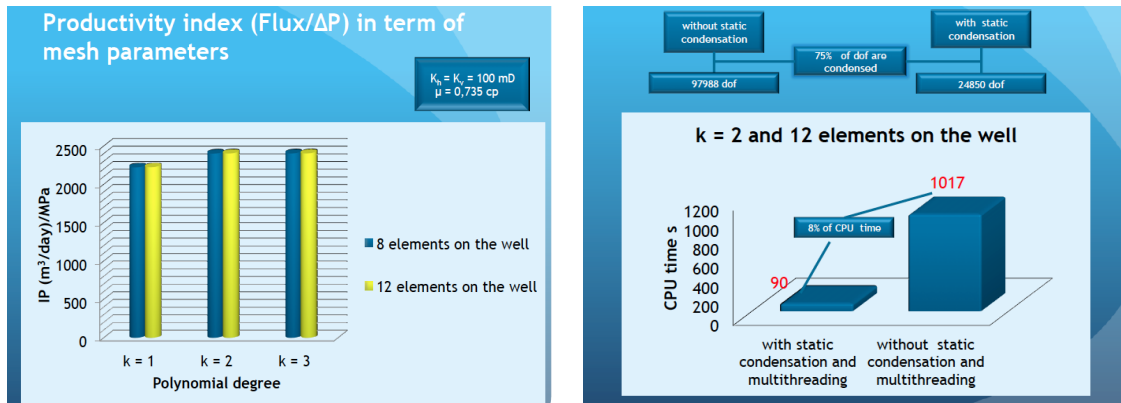


Figure 8: Problem 2: the effect of mesh parameters on the productivity index (left(side) and of static condensation and parallelization on the CPU time (right side).

work is a continuation of the research supported from FAPESP - Research Foundation of the State of São Paulo, Brazil (grant 2013/21959-4). The authors also thank the company Simworx for providing the meshes of Problem 2.

REFERENCES

- Brezzi, F., Douglas, J., Fortin, & Marini, L. D., 1987. Efficient rectangular mixed finite elements in two and three space variable, *RAIRO Modél. Math. Anal. Numér.* vol. 2, pp. 581–604.
- Brezzi, F., & Fortin, M., 1991. *Mixed and Hybrid Finite Element Methods*, Springer Series in Computational Mathematics, vol. 15, Springer-Verlag, NewYork.
- Calle, J. L. D., Devloo, P. R. B., & Gomes, S. M., 2015. Implementation of continuous hp -adaptive finite element spaces without limitations on hanging sides and distribution of approximation orders. *Comput. & Math. Appl.* vol. 70, n. 5, pp. 1051–1069.
- Castro, D. A., Devloo, P. R. B., Farias, A. M., Gomes, S. M., Siqueira D., & Durán, O., 2016a. Three dimensional hierarchical mixed finite element approximations with enhanced primal variable accuracy. *Comput. Meth. Appl. Mech. Eng.* v. 306, pp. 479–502.
- Castro, D. A., Devloo, P. R. B., Farias, A. M., Gomes, S. M., & Durán, O., 2016b. Hierarchical high order finite element bases for $H(\text{div})$ spaces based on curved meshes for two-dimensional regions or manifolds. *Journal of Computational and Applied Mathematics*, vol. 301, pp. 241–258.
- Devloo, P. R. B., Bravo, C. M. A., & Rylo, C. M. A., 2009. Systematic and generic construction of shape functions for p -adaptive meshes of multidimensional finite elements, *Comput. Methods Appl. Mech. Engrg.*, vol. 198, pp. 1716–1725.
- Devloo, P. R. B., Farias, A. M., Gomes, S. M., & Siqueira, D., 2016. Two-dimensional hp -adaptive finite element spaces for mixed formulations. *Mathematics and Computers in Simulation (Print)*, vol. 126, pp. 104–122.
- Nédélec, J. C., 1980. Mixed finite elements in \mathbb{R}^3 . *Numer. Math.*, vol. 35, pp. 315–341.
- Lucci, P. C. A., 2009. Descrição Matemática de Geometrias Curvas por Interpolação Transfinita, Master dissertation, Unicamp.

Raviart, P. A., & Thomas, J. M., 1977. A mixed finite element method for 2nd order elliptic problems. *Lect. Note Math.*, vol. 606, pp. 292-315.

Siqueira, D., Devloo, P. R. B., & Gomes, S. M., 2013. A new procedure for the construction of hierarchical high order Hdiv and Hcurl finite element spaces, *Journal of Computational and Applied Mathematics*, vol. 240, p. 204–214.